Check for updates

Original Research Article

Functional Recovery and Cellular Damage Mechanism of Mesoporous Silica Nanoparticles/Chitosan Solution/ Methylprednisolone-collagen on Nerve Injury Caused by Ketamine Overdose

Pharmacognosy Magazine
22(2) 702–713, 2026
© The Author(s) 2025
Article reuse guidelines:
in.sagepub.com/journals-permissions-india
DOI: 10.1177/09731296251360081
journals.sagepub.com/home/phm

Shuangju Liao[1], Huiqiong Huang[2] and Yuan Tang[3]

Abstract

Background: Ketamine, a commonly used anesthetic, plays a significant role during surgery, but its potential risk for neurotoxicity has drawn considerable attention.

Objectives: This study was aimed to investigate the effects of methylprednisolone (MP) loaded onto mesoporous silica nanoparticles (MSN) based on chitosan solution (CS) in ketamine overdose-induced neurotoxicity, focusing on its effects on neural function recovery and cellular damage. The goal was to provide new strategies and a theoretical foundation for the treatment of neuro injury.

Materials and Methods: MSN/CS/MP collagen (MP col) was prepared using the sol-gel method and characterized for its drug loading capacity, encapsulation efficiency, and release performance. Forty Sprague-Dawley rats were divided into five groups: control group (CG), ketamine group (KG), low concentration group (LG), medium concentration group (MG), and high concentration group (HG)). Except for the CG, the remaining groups were subjected to a ketamine-induced nerve injury model and received different concentrations of MSN/CS/MP col injections. Subsequently, the expression of key hippocampal proteins, apoptosis levels, and spatial memory were evaluated.

Results: The drug loading capacity of MSN/CS/MP col was 23.01 ± 0.51%, and the encapsulation efficiency was 95.24 ± 2.36%. Compared to CG, the escape latency was prolonged and exploratory time was shortened in the KG, LG, MG, and HG. The levels of p-Akt/Akt, Bcl-2, and PSD-95 were reduced, while the levels of Cas-3/Cas-3 and Bax were increased in the KG. The density of apoptotic cells was elevated in the KG and HG ($p<0.05$).

Conclusion: MSN/CS/MP col promotes functional recovery by regulating key proteins and reducing neuronal apoptosis, offering a novel approach for the treatment of nerve injury.

Keywords

Methylprednisolone, nanoparticles, ketamine overdose, neural injury, cellular protection

Received 24 November 2024; **revised** 20 March 2025; **accepted** 30 June 2025

Introduction

Anesthetics play an essential role in surgical procedures, making the process safer and more comfortable. However, the use of anesthetics has also raised some concerns. Ketamine, as a widely used anesthetic drug, has played an obvious role in surgery but has attracted attention due to its potential risk of neural injury (Abram et al., 2022). Studies have found that excessive ketamine use can lead to abnormal changes in neurons, especially affecting the developing nervous system more clearly (Zhang et al., 2021). Research has indicated that ketamine overdose induces hippocampal neuronal injury in developing rats, leading to cognitive dysfunction (Barreto Chang et al., 2022; Cichon et al., 2023). However, there is still no ideal treatment to address this issue.

[1]Department of Anesthesiology, West China School of Public Health and West China Fourth Hospital, Sichuan University, Chengdu, Sichuan, China
[2]Department of Anesthesiology, Chengdu Xindu District People's Hospital, Chengdu, Sichuan, China
[3]Department of Anesthesiology, Changsha Eighth Hospital, Changsha, Hunan, China

Corresponding author:
Shuangju Liao, Department of Anesthesiology, West China School of Public Health and West China Fourth Hospital, Sichuan University, Chengdu, Sichuan 610041, China.
E-mail: liaoshju@126.com

Creative Commons Non Commercial CC BY-NC: This article is distributed under the terms of the Creative Commons Attribution-NonCommercial 4.0 License (http://www.creativecommons.org/licenses/by-nc/4.0/) which permits non-Commercial use, reproduction and distribution of the work without further permission provided the original work is attributed as specified on the SAGE and Open Access pages (https://us.sagepub.com/en-us/nam/open-access-at-sage).

Methylprednisolone (MP) has been shown to protect and promote the repair and regeneration of neural tissue through its anti-inflammatory, immunosuppressive, and anti-allergic pharmacological effects in neural injury (Dubert et al., 2020; Li et al., 2022). However, the clinical use of MP is often limited by poor drug release and targeting, which restricts the effectiveness of its therapeutic impact. The application of nanotechnology in the medical field is gaining increasing attention, especially for its potential in drug delivery systems (Rabiee et al., 2021). Nanoparticles, as nano drug carriers, have shown great promise in drug delivery to the nervous system and neuroprotection due to their tiny particle size and unique surface properties (Feng et al., 2022). Studies have indicated that mesoporous silica nanoparticles (MSN) can carry and release drugs, and influence cell survival, proliferation, and function through interactions with cells, playing a role in neural function repair (Farshchi & Hasanzadeh, 2020). However, researchers have developed MSN due to potential cytotoxicity when used alone (Abdali et al., 2022; Sharma et al., 2023). Mesoporous silica nano/collagen particles, as drug delivery carriers, provide an ideal microenvironment for cell attachment and proliferation, and promote the repair and regeneration of neural tissue through biocompatibility and biodegradability (Berger et al., 2021; Sirkkunan et al., 2021). The application of nano drug-loaded particles in drug delivery offers new possibilities for the treatment of neurofunctional disorders. It brings a new perspective to the exploration of neuroprotective and reparative mechanisms (Mihaiescu et al., 2012). Chitosan solution (CS) is a natural polymer material that forms microparticles typically ranging from 1 to 1,000 nm. Due to its unique physicochemical properties, chitosan nanoparticles have attracted considerable attention in drug delivery. When combined with materials such as MSN to construct composite drug delivery systems, CS can enhance the biocompatibility of the system, as well as enable controlled drug release, targeted delivery, and reduction of toxic side effects (Poznanski et al., 2023; Zhou et al., 2023). Therefore, this study considers the use of CS as one of the components for constructing composite nanomaterials.

This study explored the application effects of MSN/CS/methylprednisolone-collagen (MP-col) (MSN/CS/MP-col) in neural injury caused by ketamine overdose, especially its impact on neural function recovery and the cellular damage mechanism. By systematically evaluating the role of this nano drug delivery system in a ketamine overdose neural injury model, it helps reveal its potential therapeutic mechanisms and provides new ideas and evidence for the intervention of neural injury after ketamine overdose.

Materials and Methods

Preparation of MSN/CS/MP-col

The method for synthesizing MSN: A total of 0.5 g of cetyltrimethylammonium bromide (Sigma–Aldrich, USA), 4 g of NaOH (Sigma–Aldrich, USA), and 240 g of deionized water was added to a flask and stirred at 300 rpm for 2 h at 80°C to ensure complete dissolution of the chemicals. Subsequently, 2.5 mL of tetraethyl orthosilicate (Sigma–Aldrich, USA) was rapidly introduced, and stirring was continued for 2 h. The resulting mixture was then filtered and washed three times with ethanol (Sigma–Aldrich, USA). Next, a 10 mg/mL NH_4NO_3-ethanol solution (Jining Fangyu Chemical Co., Ltd., China) was added, and the mixture was stirred at 80°C and 300 rpm for 6 h. The precipitate was collected and washed, yielding the MSNs.

A total of 0.675 g of MSN was added to 5 mL of CS (Sigma–Aldrich, USA) and ultrasonically dispersed for 5 min. Under a nitrogen atmosphere, 2 mL of methacrylic acid (Sigma–Aldrich, USA) was added, and the mixture was stirred at 300 rpm for 30 min. The temperature was then rapidly increased to 80°C, and 8 mg of potassium persulfate (Sigma–Aldrich, USA) was introduced, followed by stirring at 300 rpm for 2 h. Afterward, the temperature was adjusted to 50°C, and 0.1 mL of glutaraldehyde (Sigma–Aldrich, USA) was added, with stirring maintained at 300 rpm for 2 h. The resulting precipitate was collected and washed, yielding the MSN/CS composite.

Next, 5 mg of MSN/CS was added to 2 mL of a 1 mg/mL MP solution (Sigma–Aldrich, USA) and stirred at 800 rpm at room temperature for 24 h. The precipitate was collected after centrifugation at 1,000 rpm for 10 min, resulting in the MSN/CS/MP composite.

A total of 3 g of dry powdered collagen (Shanghai Guduo Biotechnology Co., Ltd., China) was gradually added to 40 mL of a 2% acrylic acid solution (Sigma–Aldrich, USA), and the mixture was stirred at 100 rpm until it was completely dissolved. The pH of the resulting solution was adjusted to neutral (pH = 7), and an appropriate amount of MSN/CS/MP was added. The final concentrations of the mixture were adjusted to 10, 25, and 50 μg/mL based on the mass of MSN. The solution was then transferred to lyophilization vials, rapidly frozen, and thoroughly ground. The resulting powder was re-dissolved in sterile physiological saline (Beijing Institute of Biological Products Co. Ltd., China), filtered, and the 10, 25, and 50 μg/mL MSN/CS/MP-col solutions were obtained. The solutions were sterilized and stored at 4°C.

Characterization of MSN, MSN/CS, and MSN/CS/MP-col

The particle size and morphology were analyzed using scanning electron microscopy (SEM, JEOL Ltd., Japan) to observe the morphology and particle size distribution of MSN and MSN/CS composites. The samples were dispersed in ethanol, dropped onto copper grids, and allowed to air dry at room temperature before testing.

The specific surface area and pore size distribution were determined by nitrogen adsorption-desorption isotherms (Brunauer–Emmett–Teller (BET) method, Micromeritics, USA) to measure the specific surface area, pore volume, and pore size distribution of MSN and MSN/CS composites.

The drug loading and encapsulation efficiency of MP in the MSN/CS/MP-col were obtained. The initial mass of MP added was determined. The mass of MP in the supernatant during the preparation of the MSN/CS/MP-col was obtained by centrifugation; the optical density (OD) at 254 nm was subjected to measurement using an ultraviolet (UV) spectrophotometer (Agilent Technologies, USA), and the mass of MP in the supernatant was calculated based on the standard curve.

An appropriate amount of MSN/CS/MP-col was added to phosphate-buffered saline (PBS) (Moregate Biotech, Australia) containing a small amount of type I collagenase (Shanghai Guduo Biotechnology Co., Ltd., China) at pH = 7.2. The mixture was incubated at 37°C and 72 rpm/min under constant temperature and oscillation. Samples were taken at different time points, and the OD at 254 nm was subjected to measurement using a UV spectrophotometer. The release of MP was calculated based on the standard curve.

Animals and Grouping

Forty male specific pathogen-free (SPF)-grade Sprague–Dawley (SD) rats (Chengdu Dasu Laboratory Animal Co., Ltd., China) were prepared, aged 7 days at the start of the experiment, and with an approximate body weight of 10–15 g. Rats at 7 days of age were selected because, during this period, the central nervous system is undergoing rapid development, making it ideal for observing the effects of drugs on neurodevelopment. Their mothers raised the rats under standard breeding conditions (23°C ± 2°C, relative humidity at 50% ± 5%, dim light with a light exposure time of 12 h/day, well-ventilated, and noise below 80 decibels) before the experiment. They were fasted and water-deprived for 6 h before the experiment. This experiment was reviewed and approved by the ethics committee of the hospital.

The 40 rats were randomly grouped, with eight rats in each group. They were designated as the control group (CG), ketamine group (KG), low concentration MSN/CS/MP-col group (LG), medium concentration MSN/CS/MP-col group (MG), and high concentration MSN/CS/MP-col group (HG). Except for the CG, the other four groups were prepared with a rat model of hippocampal neuronal injury caused by excessive ketamine.

CG: 0.1 mL of physiological saline was injected at the same time; KG: Ketamine (Fujian Gutian Pharmaceutical Co., Ltd., China) was administered at a dose of 50 mg/kg via intraperitoneal injection. LG, MG, and HG: 10, 25, and 50 μg/mL of MSN/CS/MP-col and 0.1 mL of 50 mg/kg ketamine mixture were injected via the tail vein.

Impact of MSN/CS/MP-col on Cells

Human neuroblastoma SH-SY5Y cells (Kunming Cell Bank of the Chinese Academy of Sciences, China) were subjected to culture in Dulbecco's modified Eagle medium (DMEM) (Sigma–Aldrich, USA) having 15% fetal bovine serum (FBS) (Gibco, USA) and 1% penicillin and streptomycin, at 37°C, 5% CO_2 (Shenzhen RWD Life Technology Co., Ltd., China). When the cells grew to about 80%, the supernatant was discarded, washed once with PBS, and trypsin containing ethylene diamine tetraacetic acid (Thermo Fisher Scientific, USA) was applied, centrifuged in a KS50R low-speed (Hunan Kaida Scientific Instrument Co., Ltd., China) at 1,800 r/min for 5 min. The supernatant was discarded, and DMEM with 10% FBS was applied. Cells in the log phase were collected, centrifuged (1,800 r/min for 5 min), and divided into four groups, which were stored at 4°C. 10, 25, and 50 μg/mL of MSN/CS/MP-col solutions and an equal volume of physiological saline (CG) were added, cultured in a 37°C, 5% CO_2 incubator for 24 and 72 h. Methylene blue (Sigma–Aldrich, USA) was used for hematoxylin and eosin (H&E) staining, and the morphology was observed under a light microscope.

After the end of the culture, the culture medium in the culture dish was poured off, and then 20 μL of 3-(4,5-dimethylthiazol-2-yl)-2,5-diphenyltetrazolium bromide (MTT) solution (Aladdin, USA) was applied to immerse the cells fully. The dish was placed at 37°C, 5% CO_2 for 4 h. The MTT solution in the culture dish was aspirated using a pipette (Eppendorf, Germany), and 200 μL of dimethyl sulfoxide (DMSO) (OriGen, USA) was added. 180 μL of the sample solution was added to the culture plate, and the OD at 570 nm was measured using an HBS-ScanX microplate reader (Nanjing Detie Experimental Equipment Co., Ltd., China) to assess the survival and proliferation of the cells.

Morris Water Maze (MWM) Test

When the rats reached 30 days of age, a circular MWM (Beijing Keyue Huacheng Technology Co., Ltd., China) (diameter 1.5 m, water depth 30 cm, 22°C–24°C) was prepared, with a transparent platform placed in the pool for the rats to escape onto. Multiple positioning marks were placed on the pool walls to help the rats recognize different positions. The rats were placed into the pool from different quadrants (excluding the quadrant with the platform), and the time (s) it took to climb onto the platform, that is, the escape latency, was recorded. The test was conducted for 5 consecutive days. On the 6th day, the platform was removed, and the time (s) the rats spent in the quadrant where the platform was located within 2 min, the exploration time, was recorded.

Neurological Injury Indicators (Immunoblotting Detection)

At 24 h following the experiment, the selected rats were intraperitoneally injected with 50 mg/kg pentobarbital. The hippocampal tissues of the rats were isolated on ice, cut into blocks, and fixed with 4% paraformaldehyde (Thermo Barnstead, USA) for 24 h, and stored at 4°C for later use.

The sample tissues were rinsed using PBS, and 100 μL of radio-immunoprecipitation assay lysis solution (Beijing Solarbio Technology Co., Ltd., China) was applied (4°C, half an hour). The cells or tissues were broken using a cell scraper to release the proteins. The bicinchoninic acid detection kit was used for protein quantification. 15% gel was selected for sodium dodecyl sulfate–polyacrylamide gel electrophoresis (SDS-PAGE), and proteins were loaded into the gel according to the sample concentration, with molecular weight markers added to determine the size of the proteins, and electrophoresis separation was performed. The separated proteins were transferred from the gel to the polyvinylidene fluoride (PVDF) membrane using a semi-wet transfer apparatus (in 5% skim milk powder for blocking to avoid non-specific binding). Diluted at 1:1,000, anti-p-Akt antibody (Shanghai Sig Biology Technology Co., Ltd., China), anti-Akt antibody (Shanghai Sig Biology Technology Co., Ltd., China), anti-activated Cas-3 antibody, anti-Cas-3 antibody, anti-Bax antibody, anti-Bcl-2 antibody, anti-PSD-95 antibody (Abcam, UK), and diluted at 1:500, anti-activated Cas-3 antibody, and anti-β-actin antibody were added, and incubated at 4°C overnight. The membrane was rinsed three times with PBS having Tween-20 (Sigma–Aldrich, USA), each time for 5–10 min, to remove unbound antibody. Horseradish peroxidase-labeled corresponding biotinylated secondary antibody (Sigma–Aldrich, USA) diluted at 1:5,000 was added, and incubated for 2 h. The membrane was rewashed three times. The proteins on the membrane were visualized using the enhanced chemiluminescence (ECL) reagent (Thermo Barnstead, USA), and the luminescent signals of the protein bands were observed. The APX100 digital imaging system (Olympus, Japan) was used for imaging, and the Image J software was used to quantitatively determine the OD of each protein band, which was corrected with molecular weight markers. The expression of p-Akt/Akt, anti-activated Cas-3 antibody/anti-Cas-3 antibody, anti-Bax antibody, anti-Bcl-2 antibody, and anti-PSD-95 antibody was statistically compared with the reference protein.

Apoptosis Detection

The same tissue samples used for immunoblotting detection were fixed, dehydrated in a gradient, and the hippocampal tissues were gradually soaked in ethanol solutions to remove moisture. The hippocampal tissues were embedded in paraffin, and 5-μm-thick sections were obtained using a microtome. After sectioning, the sections were deparaffinized. PBS was used for washing, and the labeling mixture was added at 37°C for 60 min, followed by another PBS wash, and the conversion solution was added at 37°C for half an hour, followed by another PBS wash. The 5-bromo-4-chloro-3-indolyl phosphate (BCIP)/nitro blue tetrazolium (NBT) alkaline phosphatase chromogenic reagent kit (Shanghai Enzyme-linked Biotechnology Co., Ltd., China) was used for H&E staining, followed by dehydration with an ethanol solution and clarification. The sections were placed on slides under a BX51 microscope (Olympus, Japan) for observation and pathological morphological assessment. ImageJ was used to compute the density of apoptotic cells.

Statistical Processing

Statistical Package for the Social Sciences (SPSS) 26.0 was employed. Measurement data were presented as mean ± standard deviation (SD) ($\bar{x} \pm s$), and a *t*-test was adopted; count data were presented by frequency or rate, and a chi-square test was adopted. The difference was statistically considerable with $p < .05$.

Results

Characterization of MSN and MSN/CS Composites

SEM images revealed that MSN particles were spherical with a uniform size distribution, approximately 100 nm in diameter. The MSN/CS composite exhibited a uniformly coated shell on the surface, with a slight increase in particle size to approximately 120 nm (Figure 1A). The surface area of MSN was relatively high (around 800 m^2/g), with an average pore size of approximately 2.5 nm. After CS coating, the specific surface area decreased to 600 m^2/g, indicating that CS partially filled the pores (Figure 1B).

Drug Loading and Release Amount of MSN/CS/MP-col

The drug loading and encapsulation efficiency of MP in the MSN/CS/MP-col were 23.01% ± 0.51% and 95.24% ± 2.36%, respectively. The *in vitro* MP release curve of the MSN/CS/MP-col suggested that the drug release exceeded 75% within 21 days, demonstrating an apparent sustained-release effect. A high drug release amount, reaching 25.25%, was observed within the first 24 h, indicating a burst release phenomenon. This was mainly due to the rapid detachment of drug particles from the surface and attachment to the nanospheres at the beginning of the release, leading to a high local drug concentration in a short period of time. The drug release amount in the 21-d *in vitro* release experiment did not reach 100% (Figure 2).

Impact of MSN/CS/MP-col on SH-SY5Y

HE staining results of SH-SY5Y cells cultured with physiological saline and 10, 25, and 50 μg/mL MSN/CS/MP-col are illustrated. In the visual fields, the majority of SH-SY5Y cells remained in a normal state. The cells using physiological saline grew in a spindle shape without any obvious abnormalities

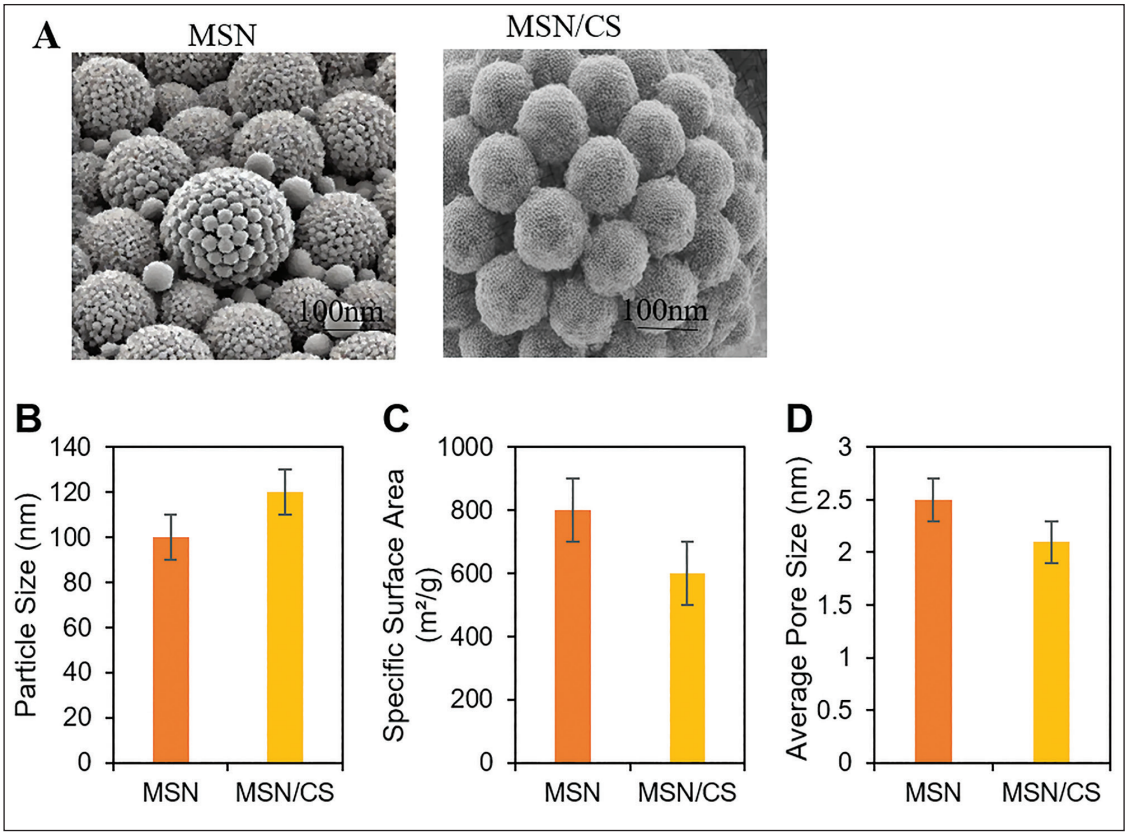


Figure 1. Scanning Electron Microscopy (SEM) Images (A), Average Particle Size (B), Specific Surface Area (C), and Average Pore Size (D).

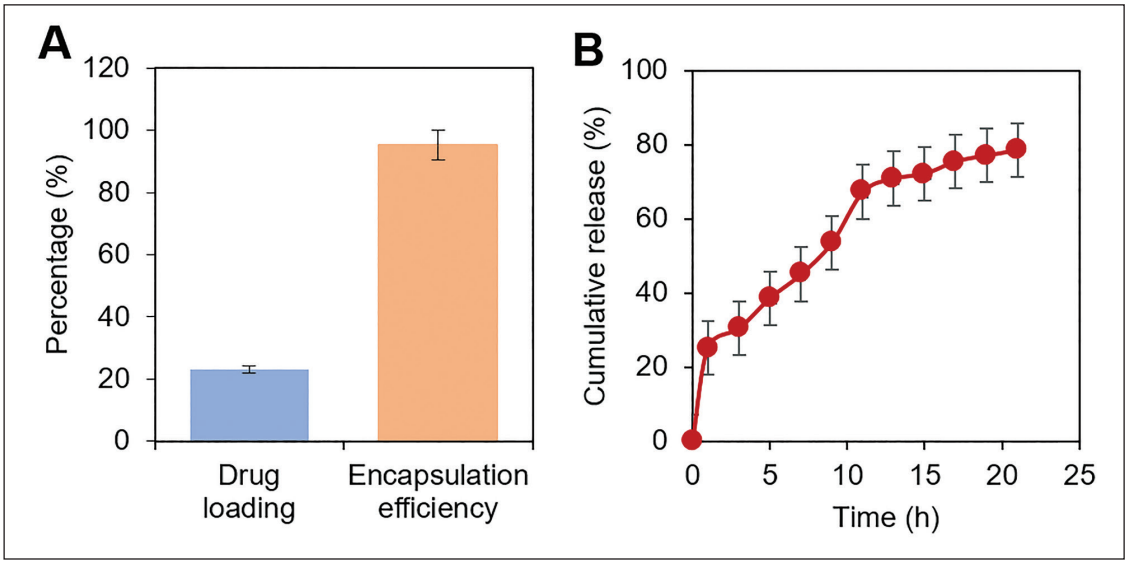


Figure 2. Drug Release Effect of Mesoporous Silica Nanoparticles (MSN)/Chitosan Solution (CS)/Methylprednisolone-collagen (MP-col). (A) Drug Loading and Encapsulation Efficiency of MSN/CS/MP-col and (B) *In Vitro* MP Release Curve of MSN/CS/MP-col.

(Figure 3A). However, the SH-SY5Y with 10 and 50 μg/mL MSN/CS/MP-col did not show a visible promotion of cell growth (Figure 3B–3C). In contrast, the SH-SY5Y with 25 μg/mL MSN/CS/MP-col not only grew in a spindle shape but also extended along the axons, showing a more active growth state (Figure 3D). The results of the MTT assay were similar to those of the H&E staining, indicating that the proliferation and activity of SH-SY5Y cells increased, and then decreased with time and concentration of MSN/CS/MP-col, reaching the highest activity at 25 μg/mL (Figure 3E).

Behavioral Results

As time and the number of experiments increased, the escape latency of all rats suggested a decreasing trend. The escape latency of the KG was visibly higher than that of the CG ($p < .05$) (Figure 4A). The escape latency of the LG, MG, and HG suggested no visible distinction compared to the CG, and there was no clear distinction in the recovery of spatial learning ability among the LG, MG, and HG ($p > .05$).

In Figure 4B, the exploration time of the KG was visibly lower than the CG. The LG, MG, and HG extended their exploration time in the same area, and the exploration duration was visibly higher than the KG, with the MG and HG showing a visibly higher degree of recovery in memory function than the LG ($p < .05$).

Contrast of Protein Expression

As against the CG, p-Akt/Akt, PSD-95, and Bcl-2 in the KG were markedly decreased; as against the KG, those were markedly increased in the LG, MG, and HG ($p < .05$). There was a similar expression among the LG, MG, and HG ($p < .05$), with the MG's indicator being the closest to that of the CG (Figure 5A–5B).

As against the CG, activated Cas-3/Cas-3 and Bax in the KG were markedly reduced; as against the KG, those were markedly raised in the LG, MG, and HG ($p < .05$). There were similarities in the expression among the LG, MG, and HG ($p < .05$), with the MG's indicator being the most similar to that of the CG (Figure 6).

Neuronal Apoptosis Detection

Apoptotic cells appeared black and were generally shrunken. From the H&E staining images, there were only a few apoptotic cells in the CG, with most cells showing a normal morphology (Figure 7A). In contrast, the KG suggested many black apoptotic cells with few normal cells (Figure 7B). In the LG, MG, and HG, as the concentration increased, the

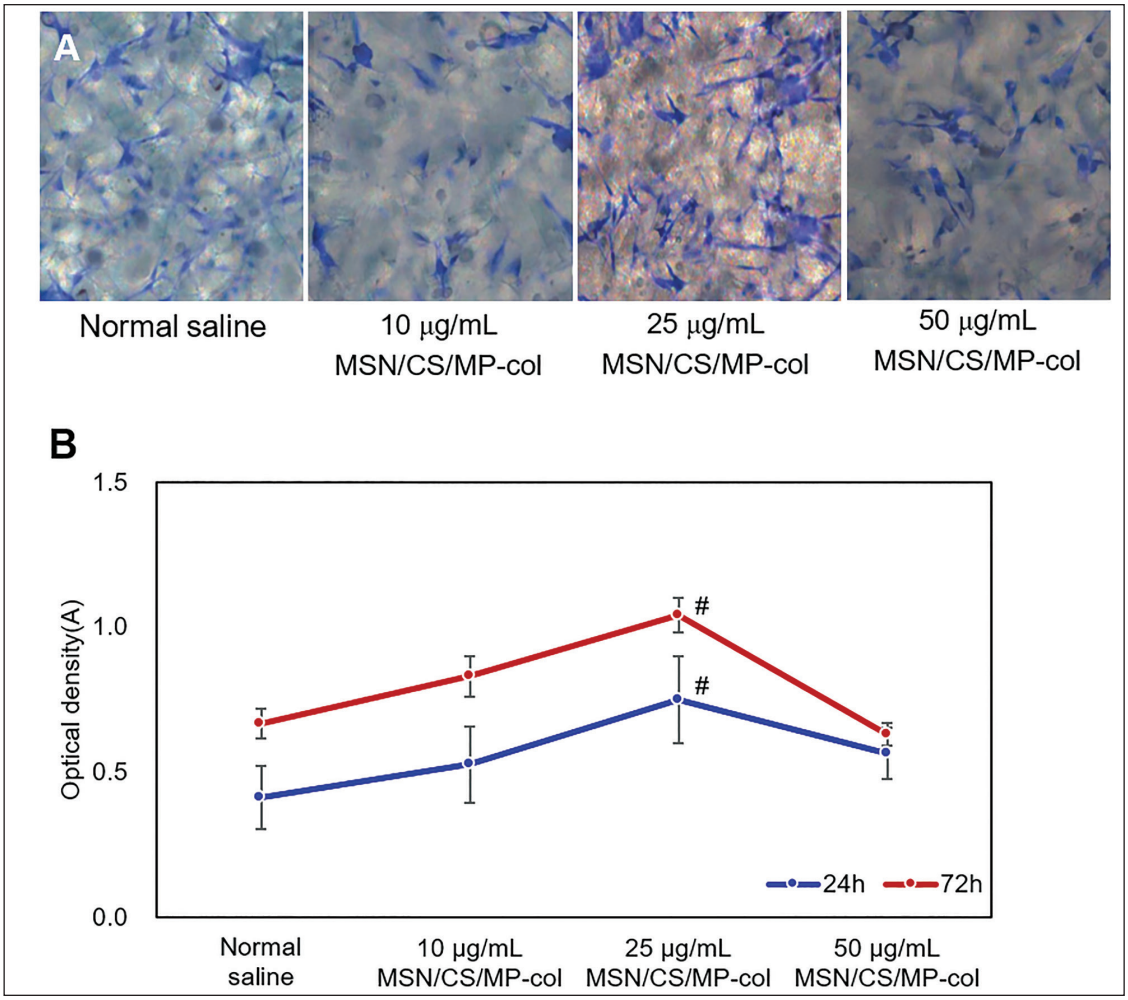


Figure 3. Hematoxylin and Eosin (H&E) Images of SH-SY5Y and 3-(4,5-Dimethylthiazol-2-yl)-2,5-Diphenyltetrazolium Bromide (MTT) Assay Results (×100). (A) MTT Assay Results and (B) Cell Proliferation Comparison at Each Time Point.

Note: # as against group A, $p < .05$.

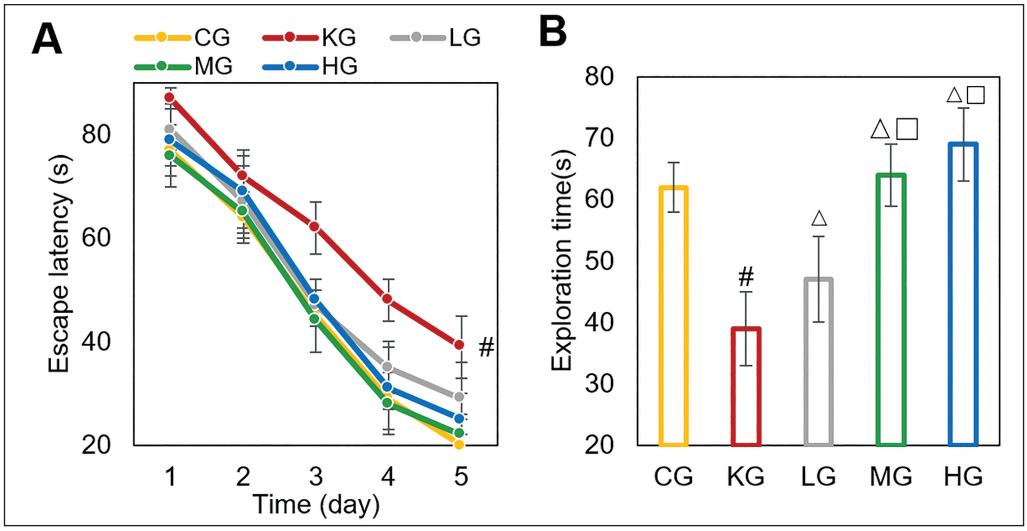


Figure 4. Contrast of Behavioral Results in Rats. (A) Escape Latency and (B) Exploration Time.

Note: # as against control group (CG), $p < .05$; △ as against ketamine group (KG), $p < .05$; □ as against low concentration MSN/CS/MP-col group (LG), $p < .05$.

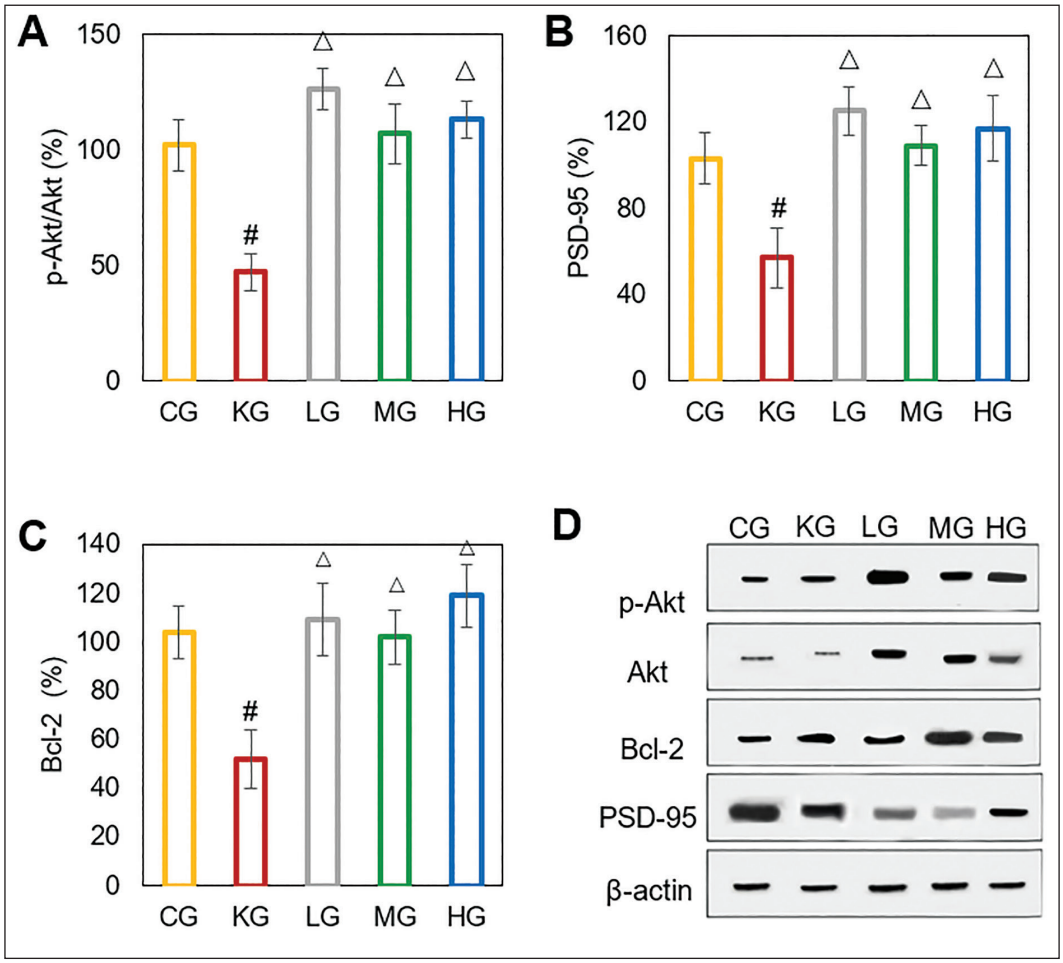


Figure 5. Protein Expression of Cell Conduction-related Pathways in Rat Hippocampal Neurons. (A) p-Akt/Akt; (B) Bcl-2; (C) PSD-95; and (D) Electrophoresis Image.

Note: # as against control group (CG), $p < .05$; △ as against ketamine group (KG), $p < .05$.

number of apoptotic cells first decreased and then increased (Figure 7C–7E), with the MG showing a reduction in apoptotic cells comparable to that of the CG.

The ImageJ software analysis results were consistent with the H&E staining. The apoptotic cell density in the KG was 3.453, markedly higher than the CG ($p < .05$). The density in the LG, MG, and HG first decreased and then increased with the concentration, and it was markedly lower in the LG and MG compared with the KG. The density was markedly lower in the HG compared with the KG ($p < .05$) (Figure 7F).

Discussion

This study explored the effects of MSN/CS/MP-col on the proliferation of SH-SY5Y, learning and memory abilities in the MWM, and apoptosis of hippocampal neurons. It assessed its reparative role in ketamine-induced neural injury through the expression of proteins. The study analyzed the drug release and sustained-release properties of the MSN/CS/MP-col, indicating that the drug-loaded microspheres effectively delayed drug release, further confirming the excellent sustained-release properties of the prepared microspheres.

In vitro experiments, the results of MTT assay and H&E staining suggested that SH-SY5Y with 10, 25, and 50 μg/mL MSN/CS/MP-col exhibited no clear toxicity, with the 25 μg/mL MSN/CS/MP-col effectively promoting the growth and proliferation of SH-SY5Y cells. Studies have suggested that MSN activates the PI3K/Akt signaling pathway by interacting with cell surface receptors. Once activated, PI3K catalyzes the conversion of PIP2 to PIP3. Activated Akt regulates the cell cycle, growth, apoptosis, and metabolism within the cell (Lee et al., 2019, 2020; Ma et al., 2022; Shao et al., 2020). Collagen particles, as part of the extracellular matrix, provide attachment and support for cells (Carvalho et al., 2021).

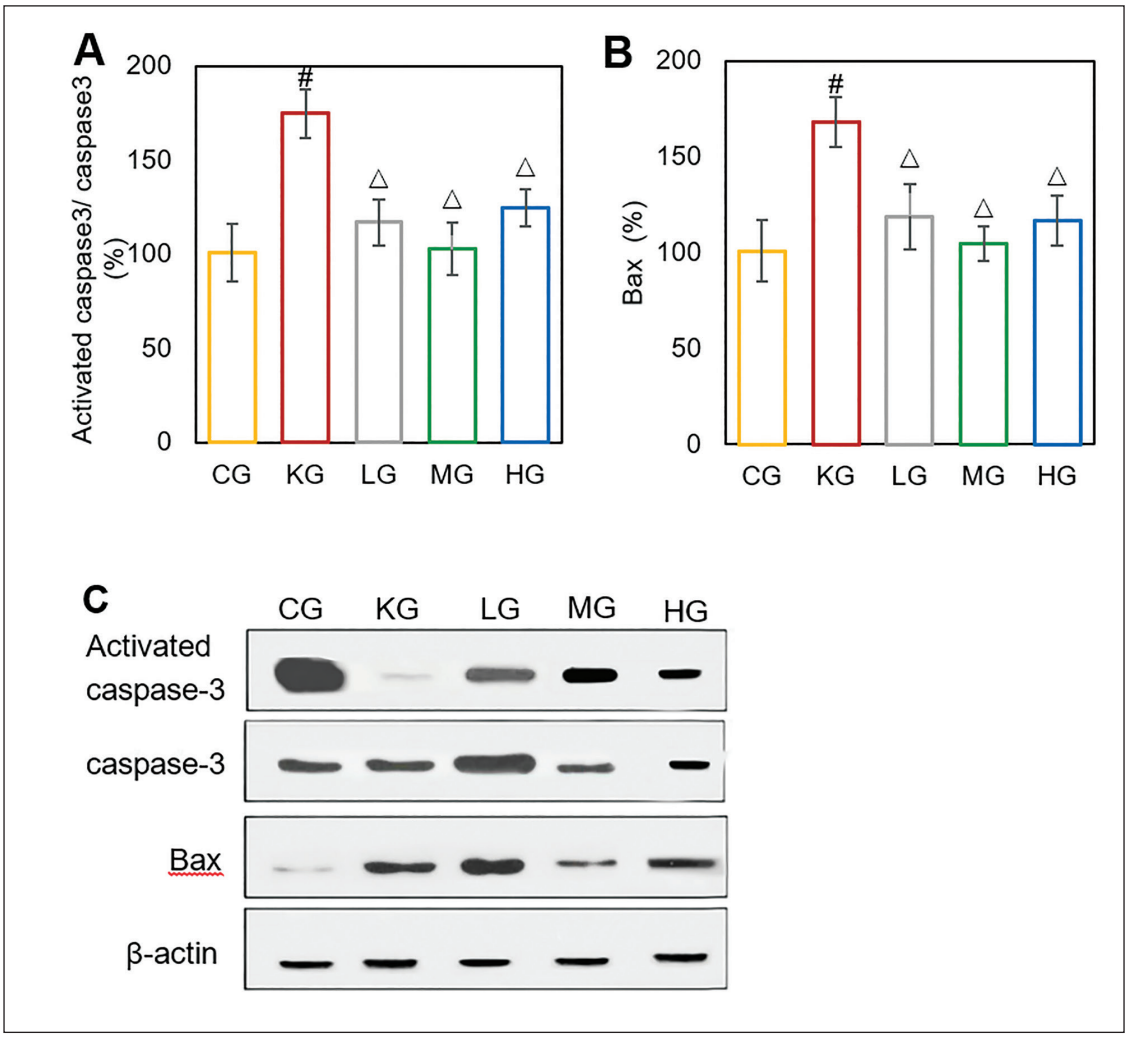


Figure 6. Protein Expression Results of Apoptosis-related Pathways in Rat Hippocampal Neurons. (A) Activated Caspase-3 (Cas-3)/ Cas-3; (B) Bax; and (C) Electrophoresis Image.

Note: # as against control group (CG), $p < .05$; △ as against ketamine group (KG), $p < .05$.

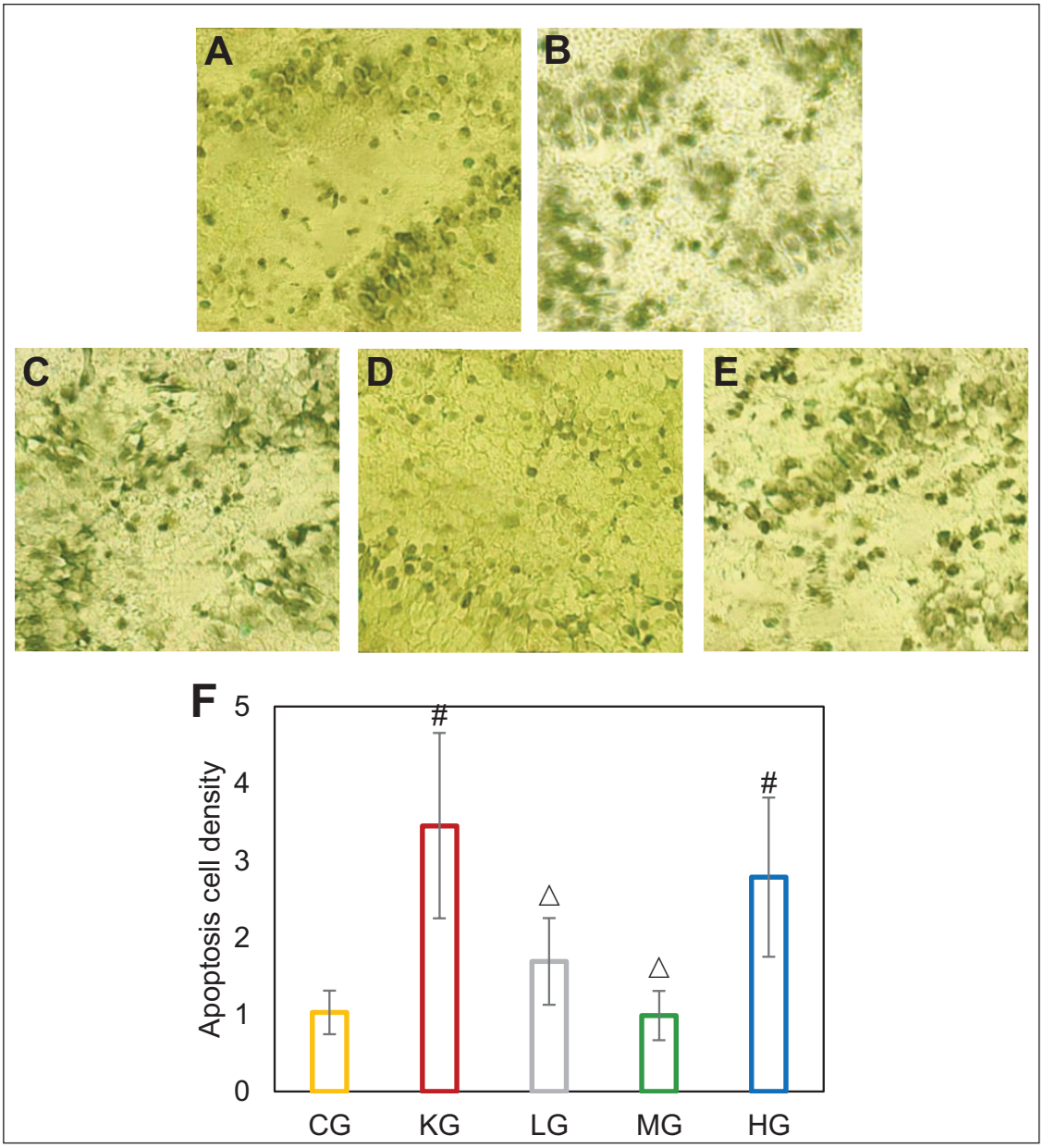


Figure 7. Effects of Different Concentrations of Mesoporous Silica Nanoparticles (MSN)/Chitosan Solution (CS)/Methylprednisolone-collagen (MP-col) on Hippocampal Neurons in Rats After Ketamine Anesthesia (×200). (A) Control Group (CG); (B) Ketamine Group (KG); (C) Low Concentration MSN/CS/MP-col Group (LG); (D) Medium Concentration MSN/CS/MP-col Group (MG); (E) High Concentration MSN/CS/MP-col Group (HG); and (F) Apoptotic Densities in Hippocampal Neurons.

Note: # as against CG, $p < .05$; △ as against KG, $p < .05$.

In vivo studies, using rats as a model, showed that the MWM test revealed that the MG and HG suggested the best recovery in spatial learning and memory functions. Research has indicated that the mechanisms of action of MP in neuroprotection are diverse, including inhibition of apoptosis, improvement of blood-brain barrier function, regulation of neural conduction, reduction of cerebral edema, promotion of neural repair, and immune modulation (Ahamed et al., 2019; Bousoulas et al., 2021; Qu et al., 2020; Wang et al., 2020). These mechanisms work synergistically to alleviate neural injury, improve neural function, enhance synaptic connections, reduce oxidative stress damage, regulate inflammatory pathways, and, thereby, restore rats' spatial learning and memory abilities. Based on this, this study focused on analyzing the regulatory effects of these nanoparticles on p-Akt/Akt and others in the rat model. The results suggested that nanoparticles of different concentrations markedly raised the expression of these indicators, primarily the effect of

25 μg/mL MSN/CS/MP-col, which was closest to that of the CG. The results of this study are consistent with existing literature. The Akt signaling pathway plays a key role in the survival of neural cells, while PSD-95 and Bcl-2 are closely related to the stability and anti-apoptotic characteristics of neurons (Gholinejad et al., 2019; Go et al., 2023; Lee et al., 2024; Li et al., 2024). Activated Cas-3 is a key apoptotic execution enzyme, and when activated Cas-3/Cas-3 decreases, it means that the activity of the apoptotic pathway is reduced, leading to the inhibition of cell apoptosis (Kong et al., 2019; Tang et al., 2023). Bax promotes apoptosis, and when Bax decreases, it helps maintain the survival state of cells (Gu et al., 2022; He et al., 2020; Lu et al., 2022; Zhao et al., 2020). The molecular mechanisms mentioned in this literature are consistent with the neuroprotective effects of MSN/CS/MP-col found in this study. This study fills the gap regarding the specific mechanisms of action of MSN/CS/MP-col in ketamine-induced neural injury. This study also found that apoptotic cells in the nanoparticle treatment group suggested a trend of decreasing and then increasing with concentration changes, especially at 25 μg/mL, where the number of apoptotic cells markedly decreased, approaching the level of the CG. This result provides a new perspective for exploring the potential role of nanoparticles in neuroprotection. The comparison with existing literature shows that the results of this study are, to some extent, consistent with the previously reported protective effects of nanoparticles on neurons. MSN/CS/MP-col reduces cell apoptosis by regulating the apoptotic pathways (Distasi et al., 2019; Yuan et al., 2022). However, this study further found that the effect of different concentrations of nanoparticles on cell apoptosis is not linear but presents a complex relationship of decreasing and then increasing, filling the gap in the literature regarding the dose-dependent effects of nanoparticles.

This study innovatively employed a multi-level *in vitro* and *in vivo* experimental design, including MTT assays, H&E staining at the cellular level, and MWM tests in rat models, providing robust evidence to validate the neuroprotective effects of MSN/CS/MP-col. Additionally, a detailed mechanistic exploration of MSN/CS/MP-col's role in the PI3K/Akt signaling pathway was conducted, revealing its potential mechanisms in alleviating neural injury and promoting nerve repair. Furthermore, this research fills the gap in understanding the specific mechanisms of MSN/CS/MP-col in repairing ketamine-induced neural damage, thus broadening the application of nanoparticles in neuroprotection.

However, this study has certain limitations. First, although the effects of MSN/CS/MP-col were explored through cellular and animal experiments, the long-term effects and potential side effects were not further investigated, which are crucial for clinical translation. Second, the *in vivo* experiments predominantly relied on rat models, and further validation is needed to assess their efficacy and safety in human neural injury. Additionally, the dose-dependent effects of nanoparticles exhibit a complex relationship. Although MSN/CS/MP-col showed optimal performance at 25 μg/mL, the effects at varying concentrations remain unclear, and future research should investigate the pharmacological effects at different dosages. Lastly, while MSN/CS/MP-col demonstrated positive effects in neural damage repair, the specific intracellular mechanisms still require further cytological and molecular studies.

In summary, although this study provides compelling evidence of the potential neuroprotective effects of MSN/CS/MP-col, further research is necessary to address the aforementioned limitations, particularly regarding long-term effects, dose dependency, and its application in human neural injury.

Conclusion

This study demonstrates that MSN/CS/MP-col has visible neuroprotective and functional recovery effects in neural injury caused by ketamine overdose. MSN/CS/MP-col effectively promotes the damaged neurons' survival and functional recovery. In addition, under low- and medium-concentration treatment conditions, MSN/CS/MP-col markedly reduced the level of cell apoptosis, showing potential application value in reducing neuronal injury caused by excessive anesthesia. These findings offer empirical support for the possible application of MSN/CS/MP-col to treat neural injury caused by excessive anesthesia.

Abbreviations

Cas-3: Caspase-3; CG: Control group; CS: Chitosan solution; DMEM: Dulbecco's modified Eagle medium; FBS: Fetal bovine serum; HG: High concentration MSN/CS/MP-col group; KG: Ketamine group; LG: Low concentration MSN/CS/MP-col group; MG: Medium concentration MSN/CS/MP-col group; MP: Methylprednisolone; MP-col: Methylprednisolone-collagen; MSN: Mesoporous silica nanoparticles; MWM: Morris water maze; PBS: Phosphate-buffered saline; PVDF: Polyvinylidene fluoride.

Authors Contribution

Conception and study design: Shuangju Liao; data acquisition and analysis: Shuangju Liao, Huiqiong Huang, and Yuan Tang; manuscript draft, editing, and revision: Shuangju Liao and Huiqiong Huang. All authors approved the final manuscript.

Declaration of Conflicting Interests

The authors declared no potential conflicts of interest with respect to the research, authorship, and/or publication of this article.

Ethical Approval and Informed Consent

This animal study protocol was approved by the Ethics Committee of West China Fourth Hospital of Sichuan University, in compliance with Chinese national guidelines for the care and use of animals.

Funding

The authors received no financial support for the research, authorship, and/or publication of this article.

ORCID iD

Shuangju Liao https://orcid.org/0009-0002-7006-2445

References

Abdali, Z., Aminzare, M., Chow, A., & Dorval Courchesne, N. M. (2022). Bacterial collagen-templated synthesis and assembly of inorganic particles. *Biomedical Materials*, *18* (1). https://doi.org/10.1088/1748-605X/ac9d7b

Abram, S. V., Roach, B. J., Fryer, S. L., Calhoun, V. D., Preda, A., van Erp, T. G. M., Bustillo, J. R., Lim, K. O., Loewy, R. L., Stuart, B. K., Krystal, J. H., Ford, J. M., & Mathalon, D. H. (2022). Validation of ketamine as a pharmacological model of thalamic dysconnectivity across the illness course of schizophrenia. *Molecular Psychiatry*, *27*(5), 2448–2456. https://doi.org/10.1038/s41380-022-01502-0

Ahamed, M., Akhtar, M. J., & Alhadlaq, H. A. (2019). Co-exposure to SiO2 nanoparticles and arsenic induced augmentation of oxidative stress and mitochondria-dependent apoptosis in human cells. *International Journal of Environmental Research and Public Health*, *16*(17), 3199. https://doi.org/10.3390/ijerph16173199

Barreto Chang, O. L., Kreuzer, M., Morgen, D. F., Possin, K. L., & García, P. S. (2022). Ketamine-associated intraoperative electroencephalographic signatures of elderly patients with and without preoperative cognitive impairment. *Anesthesia and Analgesia*, *135*(4), 683–692. https://doi.org/10.1213/ANE.0000000000005875

Berger, A. G., Chou, J. J., & Hammond, P. T. (2021). Approaches to modulate the chronic wound environment using localized nucleic acid delivery. *Advances in Wound Care*, *10*(9), 503–528. https://doi.org/10.1089/wound.2020.1167

Bousoulas, P., Papakonstantinopoulos, C., Kitsios, S., Moustakas, K., Sirakoulis, G. C., & Tsoukalas, D. (2021). Emulating artificial synaptic plasticity characteristics from SiO2-based conductive bridge memories with Pt nanoparticles. *Micromachines*, *12*(3), 306. https://doi.org/10.3390/mi12030306

Carvalho, M. S., Cabral, J. M. S., da Silva, C. L., & Vashishth, D. (2021). Bone matrix non-collagenous proteins in tissue engineering: Creating new bone by mimicking the extracellular matrix. *Polymers*, *13*(7), 1095. https://doi.org/10.3390/polym13071095

Cichon, J., Wasilczuk, A. Z., Looger, L. L., Contreras, D., Kelz, M. B., & Proekt, A. (2023). Ketamine triggers a switch in excitatory neuronal activity across neocortex. *Nature Neuroscience*, *26*(1), 39–52. https://doi.org/10.1038/s41593-022-01203-5

Distasi, C., Dionisi, M., Ruffinatti, F. A., Gilardino, A., Bardini, R., Antoniotti, S., Catalano, F., Bassino, E., Munaron, L., Martra, G., & Lovisolo, D. (2019). The interaction of SiO2 nanoparticles with the neuronal cell membrane: Activation of ionic channels and calcium influx. *Nanomedicine*, *14*(5), 575–594. https://doi.org/10.2217/nnm-2018-0256

Dubert, M., Le Toriellec, E., Croisille, L., Thomas, L., Ducreux, M., Froissart, A., Herbrecht, R., Lebrun-Vignes, B., Marolleau, J. P., Méric, J. B., Mahevas, M., Michel, M., & Bierling, P. (2020). Methylprednisolone-induced immune thrombocytopenia. *American Journal of Hematology*, *95*(1), E13–E16. https://doi.org/10.1002/ajh.25645

Farshchi, F., & Hasanzadeh, M. (2020). Nanomaterial based aptasensing of prostate specific antigen (PSA): Recent progress and challenges in efficient diagnosis of prostate cancer using biomedicine. *Biomedicine & Pharmacotherapy = Biomedecine & Pharmacotherapie*, *132*, 110878. https://doi.org/10.1016/j.biopha.2020.110878

Feng, P., Jia, J., Peng, S., Shuai, Y., Pan, H., Bai, X., & Shuai, C. (2022). Transcrystalline growth of PLLA on carbon fiber grafted with nano-SiO2 towards boosting interfacial bonding in bone scaffold. *Biomaterials Research*, *26*(1), 2. https://doi.org/10.1186/s40824-021-00248-0

Gholinejad, Z., Khadem Ansari, M. H., & Rasmi, Y. (2019). Titanium dioxide nanoparticles induce endothelial cell apoptosis via cell membrane oxidative damage and p38, PI3K/Akt, NF-κB signaling pathways modulation. *Journal of Trace Elements in Medicine and Biology*, *54*, 27–35. https://doi.org/10.1016/j.jtemb.2019.03.008

Go, M. J., Kim, J. M., Lee, H. L., Kim, T. Y., Joo, S. G., Kim, J. H., Lee, H. S., Kim, D. O., & Heo, H. J. (2023). Anti-amnesia-like effect of *Pinus densiflora* extract by improving apoptosis and neuroinflammation on trimethyltin-induced ICR mice. *International Journal of Molecular Sciences*, *24*(18), 14084. https://doi.org/10.3390/ijms241814084

Gu, Q., Duan, K., Petralia, R. S., Wang, Y. X., & Li, Z. (2022). BAX regulates dendritic spine development via mitochondrial fusion. *Neuroscience Research*, *182*, 25–31. https://doi.org/10.1016/j.neures.2022.06.002

He, Y., Jiang, K., & Zhao, X. (2020). Taraxasterol protects hippocampal neurons from oxygen-glucose deprivation-induced injury through activation of Nrf2 signalling pathway. *Artificial Cells, Nanomedicine, and Biotechnology*, *48*(1), 252–258. https://doi.org/10.1080/21691401.2019.1699831

Kong, C., Miao, F., Wu, Y., & Wang, T. (2019). Oxycodone suppresses the apoptosis of hippocampal neurons induced by oxygen-glucose deprivation/recovery through caspase-dependent and caspase-independent pathways via κ- and δ-opioid receptors in rats. *Brain Research*, *1721*, 146319. https://doi.org/10.1016/j.brainres.2019.146319

Lee, H. L., Kim, J. M., Go, M. J., Lee, H. S., Kim, J. H., & Heo, H. J. (2024). Fermented *Protaetia brevitarsis* larvae improves neurotoxicity in chronic ethanol-induced-dementia mice via suppressing AKT and NF-κB signaling pathway. *International Journal of Molecular Sciences*, *25*(5), 2629. https://doi.org/10.3390/ijms25052629

Lee, K., Lee, J., Kwak, M., Cho, Y. L., Hwang, B., Cho, M. J., Lee, N. G., Park, J., Lee, S. H., Park, J. G., Kim, Y. G., Kim, J. S., Han, T. S., Cho, H. S., Park, Y. J., Lee, S. J., Lee, H. G., Kim, W. K., Jeung, I. C., … Min, J. K. (2019). Two distinct cellular pathways leading to endothelial cell cytotoxicity by silica nanoparticle size. *Journal of Nanobiotechnology*, *17*(1), 24. https://doi.org/10.1186/s12951-019-0456-4

Lee, K. I., Su, C. C., Fang, K. M., Wu, C. C., Wu, C. T., & Chen, Y. W. (2020). Ultrafine silicon dioxide nanoparticles cause lung epithelial cells apoptosis via oxidative stress-activated PI3K/Akt-mediated mitochondria- and endoplasmic reticulum stress-dependent signaling pathways. *Scientific Reports*, *10*(1), 9928. https://doi.org/10.1038/s41598-020-66644-z

Li, M., Liu, Y., Sun, M., Yang, Y., Zhang, L., Liu, Y., Li, F., & Liu, H. (2024). SEP-363856 exerts neuroprotection through the PI3K/AKT/GSK-3β signaling pathway in a dual-hit neurodevelopmental model of schizophrenia-like mice. *Drug Development Research*, *85*(4), e22225. https://doi.org/10.1002/ddr.22225

Li, X., Song, B., Teng, X., Li, Y., Yang, Y., & Zhu, J. (2022). Low dose of methylprednisolone for pain and immune function after thoracic surgery. *The Annals of Thoracic Surgery*, *113*(4), 1325–1332. https://doi.org/10.1016/j.athoracsur.2021.04.055

Lu, Q., Zhang, Y., Zhao, C., Zhang, H., Pu, Y., & Yin, L. (2022). Copper induces oxidative stress and apoptosis of hippocampal neuron via pCREB/BDNF/ and Nrf2/HO-1/NQO1 pathway. *Journal of Applied Toxicology*, *42*(4), 694–705. https://doi.org/10.1002/jat.4252

Ma, L., Wei, J., Zeng, Y., Liu, J., Xiao, E., Kang, Y., & Kang, Y. (2022). Mesenchymal stem cell-originated exosomal circDIDO1 suppresses hepatic stellate cell activation by miR-141-3p/PTEN/AKT pathway in human liver fibrosis. *Drug Delivery*, *29*(1), 440–453. https://doi.org/10.1080/10717544.2022.2030428

Mihaiescu, D., Grumezescu, A., Buteica, A., Mogosanu, D., Balaure, P., Mihaiescu, O., Traistaru, V., & Vasile, B. (2012). Bioassay and electrochemical evaluation of controlled release behavior of cephalosporins from magnetic nanoparticles. *Digest Journal of Nanomaterials and Biostructures*, *7*, 253–260.

Poznanski, P., Hameed, A., & Orczyk, W. (2023). Chitosan and chitosan nanoparticles: Parameters enhancing antifungal activity. *Molecules (Basel, Switzerland)*, *28*(7), 2996. https://doi.org/10.3390/molecules28072996

Qu, M., Jiang, X., Zhou, X., Wang, C., Wu, Q., Ren, L., Zhu, J., Zhu, S., Tebon, P., Sun, W., & Khademhosseini, A. (2020). Stimuli-responsive delivery of growth factors for tissue engineering. *Advanced Healthcare Materials*, *9*(7), e1901714. https://doi.org/10.1002/adhm.201901714

Rabiee, N., Khatami, M., Jamalipour Soufi, G., Fatahi, Y., Iravani, S., & Varma, R. S. (2021). Diatoms with invaluable applications in nanotechnology, biotechnology, and biomedicine: Recent advances. *ACS Biomaterials Science & Engineering*, *7*(7), 3053–3068. https://doi.org/10.1021/acsbiomaterials.1c00475

Shao, L., Wang, R., Sun, Y., Yue, Z., Sun, H., Wang, X., Wang, P., Sun, G., Hu, J., Sun, H., Xie, S., & Li, Y. (2020). Delivery of microRNA-let-7c-5p by biodegradable silica nanoparticles suppresses human cervical carcinoma cell proliferation and migration. *Journal of Biomedical Nanotechnology*, *16*(11), 1600–1611. https://doi.org/10.1166/jbn.2020.2989

Sharma, A., Kokil, G. R., He, Y., Lowe, B., Salam, A., Altalhi, T. A., Ye, Q., & Kumeria, T. (2023). Inorganic/organic combination: Inorganic particles/polymer composites for tissue engineering applications. *Bioactive Materials*, *24*, 535–550. https://doi.org/10.1016/j.bioactmat.2023.01.003

Sirkkunan, D. S., Muhamad, F., & Pingguan-Murphy, B. (2021). Application of "magnetic anchors" to align collagen fibres for axonal guidance. *Gels (Basel, Switzerland)*, *7*(4), 154. https://doi.org/10.3390/gels7040154

Tang, T., Lian, Y., Lu, L., Xu, S., & Yu, Z. (2023). Crosstalk between activating transcription factor 6 and the inositol-requiring enzyme 1-X-box binding protein 1 pathway in oxygen-glucose deprivation/reoxygenation-injured HT22 cells. *Zhonghua Wei Zhong Bing Ji Jiu Yi Xue*, *35*(3), 278–286. https://doi.org/10.3760/cma.j.cn121430-20230228-00115

Wang, M., Li, J., Dong, S., Cai, X., Simaiti, A., Yang, X., Zhu, X., Luo, J., Jiang, L. H., Du, B., Yu, P., & Yang, W. (2020). Silica nanoparticles induce lung inflammation in mice via ROS/PARP/TRPM2 signaling-mediated lysosome impairment and autophagy dysfunction. *Particle and Fibre Toxicology*, *17*(1), 23. https://doi.org/10.1186/s12989-020-00353-3

Yuan, S., Wei, Y., Wang, X., Liu, S., Zhang, H., & Yuan, S. (2022). Mechanistic study of the adsorption and penetration of modified SiO2 nanoparticles on cellular membrane. *Chemosphere*, *294*, 133793. https://doi.org/10.1016/j.chemosphere.2022.133793

Zhang, N., Yao, L., Wang, P., & Liu, Z. (2021). Immunoregulation and antidepressant effect of ketamine. *Translational Neuroscience*, *12*(1), 218–236. https://doi.org/10.1515/tnsci-2020-0167

Zhao, J., Wang, M., Liu, W., Ma, Z., & Wu, J. (2020). Activation of cannabinoid receptor 2 protects rat hippocampal neurons against Aβ-induced neuronal toxicity. *Neuroscience Letters*, *735*, 135207. https://doi.org/10.1016/j.neulet.2020.135207

Zhou, X., Zhang, W., Zhao, L., Gao, S., Liu, T., & Yu, D. (2023). Immobilization of lipase in chitosan-mesoporous silica material and pore size adjustment. *International Journal of Biological Macromolecules*, *235*, 123789. https://doi.org/10.1016/j.ijbiomac.2023.123789